J|A|C|S ARTICLES

Published on Web 03/24/2009

Process of Accumulation of Metal Ions on the Interior Surface of apo-Ferritin: Crystal Structures of a Series of apo-Ferritins Containing Variable Quantities of Pd(II) Ions

Takafumi Ueno,*[,†,‡] Mizue Abe,[§] Kunio Hirata,[||,⊥] Satoshi Abe,[†] Masako Suzuki,[§] Nobutaka Shimizu,[⊥] Masaki Yamamoto,[||,⊥] Masaki Takata,[||,⊥,#] and Yoshihito Watanabe*[,▽]

Institute for Integrated Cell-Material Sciences (iCeMS), Funai Center, Kyoto University, Katsura, Nishikyo-ku, Kyoto 615-8510, Japan, PRESTO, Japan Science and Technology Agency (JST) Honcho, Kawaguchi, Saitama 332-0012, Japan, Department of Chemistry, Graduate School of Science, Nagoya University, Furo-cho, Nagoya 464-8602, Japan, RIKEN SPring-8 Center, Sayo-gun, Hyogo 679-5198, Japan, Japan Synchrotron Radiation Research Institute, Sayo-gun, Hyogo 679-5198, Japan, The University of Tokyo and CREST, JST, and Research Center for Materials Science, Nagoya University, Furo-cho, Nagoya 464-8602, Japan

Received August 26, 2008; E-mail: taka@sbchem.kyoto-u.ac.jp; yoshi@nucc.cc.nagoya-u.ac.jp

Abstract: Accumulation of metal ions on protein surfaces is an important subject in the field of materials science because these processes are applicable to the preparation of bioinspired inorganic materials. While previous studies related to this subject have focused on the preparation of nanomaterials using protein scaffolds, the detailed processes of metal ion deposition and metal core formation on a protein surface require clarification. Elucidation of the coordination structures of multinuclear metal binding sites on proteins at an early stage as well as intermediate and fully occupied stages of the metal ion deposition will help us to understand the reaction mechanisms so that desirable inorganic materials can be prepared using protein scaffolds. In this Article, we report on the detailed processes of accumulation of Pd(II) ions demonstrated by a series of X-ray crystal structural analyses of apo-ferritin (apo-Fr), an iron storage protein, containing different amounts of Pd(II) ions in the protein cage. We have identified the specific binding sites of Pd(II) ions and analyzed the dynamic changes in the coordination structure by a combination of the crystal structures and ICP quantitative analyses of apo-Fr containing low, intermediate, and high content of Pd(II) ions. Our studies on Pd^{II}•apo-Frs provide intriguing implications for the preparation of many other inorganic materials using protein surfaces.

Introduction

Synthesis of inorganic materials using proteins is a subject that has gained much attention in the field of nanomaterials science.[1−10] In particular, caged protein assemblies have been employed as molecular templates to synthesize metallic nanoparticles with regulated sizes, compositions, and morphologies. Ferritin (Fr) is one of the most widely studied caged protein assemblies with respect to both applications for synthesis of nanomaterials and fundamental studies for biomineralization.[9,11] Fr utilizes its large protein cage consisting of 24 subunits with a molecular weight greater than 480 kDa for the biological role of iron storage.[12,13] Thousands of iron ions can be accommodated by oxidation of Fe(II) to Fe(III) to form iron oxide minerals in the 8 nm diameter Fr cage. It is known that several metal ions other than iron and small organic molecules can be accumulated in the cage.[13−16] The protein cage thus represents

† iCeMS, Kyoto University.
‡ PRESTO, Japan Science and Technology Agency (JST).
§ Department of Chemistry, Nagoya University.
|| RIKEN SPring-8 Center.
⊥ Japan Synchrotron Radiation Research Institute.
The University of Tokyo and CREST, JST.
▽ Research Center for Materials Science, Nagoya University.

(1) Douglas, T.; Young, M. *Nature* **1998**, *393*, 152–155.
(2) Meldrum, F. C.; Wade, V. J.; Nimmo, D. L.; Heywood, B. R.; Mann, S. *Nature* **1991**, *349*, 684–687.
(3) Mao, C. B.; Solis, D. J.; Reiss, B. D.; Kottmann, S. T.; Sweeney, R. Y.; Hayhurst, A.; Georgiou, G.; Iverson, B.; Belcher, A. M. *Science* **2004**, *303*, 213–217.
(4) Shenton, W.; Pum, D.; Sleytr, U. B.; Mann, S. *Nature* **1997**, *389*, 585–587.
(5) McMillan, R. A.; Paavola, C. D.; Howard, J.; Chan, S. L.; Zaluzec, N. J.; Trent, J. D. *Nat. Mater.* **2002**, *1*, 247–252.
(6) Ishii, D.; Kinbara, K.; Ishida, Y.; Ishii, N.; Okochi, M.; Yohda, M.; Aida, T. *Nature* **2003**, *423*, 628–632.
(7) Kramer, R. M.; Li, C.; Carter, D. C.; Stone, M. O.; Naik, R. R. *J. Am. Chem. Soc.* **2004**, *126*, 13282–13286.
(8) Vriezema, D. M.; Aragones, M. C.; Elemans, J.; Cornelissen, J.; Rowan, A. E.; Nolte, R. J. M. *Chem. Rev.* **2005**, *105*, 1445–1489.
(9) Uchida, M.; Klem, M. T.; Allen, M.; Suci, P.; Flenniken, M.; Gillitzer, E.; Varpness, Z.; Liepold, L. O.; Young, M.; Douglas, T. *Adv. Mater.* **2007**, *19*, 1025–1042.
(10) *Handbook of Biomineralization*; Behrens, P., Baeuerlein, E., Eds.; Wiley-VCH: Weinheim, 2007; Vol. 2.
(11) Mann, S. *Biomineralization: Principles and Concepts in Bioinorganic Materials Chemistry*; Oxford University Press: Oxford, 2001; Vol. 5.
(12) Liu, X. F.; Theil, E. C. *Acc. Chem. Res.* **2005**, *38*, 167–175.
(13) Harrison, P. M.; Arosio, P. *Biochim. Biophys. Acta* **1996**, *1275*, 161–203.
(14) d'Estaintot, B. L.; Paolo, S.; Granier, T.; Gallois, B.; Chevalier, J. M.; Precigoux, G.; Levi, S.; Arosio, P. *J. Mol. Biol.* **2004**, *340*, 277–293.

 10.1021/ja806688s CCC: $40.75

a promising nanoreactor for preparation of various inorganic materials such as quantum dots, metal oxides, and metal nanoparticles.[2,7,17−27] Previous studies on these subjects have focused on the preparation of nanomaterials using metal ions and proteins rather than investigating accumulation mechanisms. While early studies on the nucleation mechanism of iron ions on the internal surfaces of apo-Frs were attempted by X-ray crystallography, site-directed mutagenesis, metal substitution, and theoretical calculations,[10,15,28−40] the detailed processes of other metal ion deposition and metal core formation remain obscure. Recently, Domínguez-Vera and co-workers have reported insights into the structural influences on the mechanism of copper core formation in apo-Fr on the basis of X-ray absorption spectra and small-angle X-ray scattering.[41] In addition, it has also been reported that the small metal clusters are formed in the iron storage,[42] iron binding,[43] and W/Mo storage proteins[44] as well as several peptide fragments having high affinities for metal ions,[45] which are conserved in native metalloproteins. However, details of the dynamic process of metal ion coordination on protein surfaces or peptide fragments have yet to be clarified. Therefore, determination of the coordination structures of multinuclear metal binding sites on the internal surface of apo-Fr is crucial for understanding the process of accumulation of metal ions on protein surfaces. The results will help not only the preparation of nanomaterials but also an in-depth understanding of fundamental roles of protein−metal ion interactions in biomineralization processes. We have already reported on the preparation of a Pd nanoparticle in the native horse spleen apo-Fr (apo-HSFr) cage with a narrow size distribution and that these nanoparticles are capable of catalyzing hydrogenation of olefins.[27] It is thought that the Pd nanoparticles that have a monodispersed size distribution are formed in apo-HSFr cages as a result of coordination of a limited number of Pd(II) ions to the internal surface of apo-HSFr. Moreover, crystal structures of apo-recombinant horse L-ferritin (apo-rHLFr) containing Pd organometal complexes or Cd ions indicate that apo-rHLFr is useful to determine coordination geometries of many metal ions deposited in the apo-rHLFr cage.[36,46] The crystal structures have revealed that a particular ferritin sequence containing a Cys residue at position 48, which is found only in HLFr, plays a crucial role for coordination to these metal ions.[36,46] In this work, we report a series of crystal structures of apo-rHLFr composites containing low, intermediate, and high content of Pd(II) ions (**Pd^{II}·apo-rHLFrs**) in combination with quantitative analyses. These composites are thought to represent intermediate states of Pd(II) ion accumulation in the apo-Fr cage. Moreover, to confirm high-affinity Pd(II) sites that play a role in localizing Pd(II) ions, we have determined the structure of the mutant (apo-H49A-rHLFr) with high content of Pd(II) ions. These structures could be good models for the binding and nucleation of various metal ions on protein surfaces.

Results and Discussion

Preparation and Crystallization of apo-rHLFrs and apo-H49A-rHLFr Containing Pd(II) Ions. We have prepared composites of apo-rHLFr (recombinant L-chain apo-Fr from horse liver) containing low, intermediate, and high content of Pd(II) ions (**L-Pd^{II}·apo-rHLFr**, **I-Pd^{II}·apo-rHLFr**, and **H-Pd^{II}·apo-rHLFr**) by treating apo-Fr with 50, 100, and 200 equiv of $K_2Pd^{II}Cl_4$, respectively, as reported previously (and see Supporting Information).[27] The samples were purified by size exclusion chromatography (ÄKTA Superdex G-200) after stirring the reaction mixtures for 30 min at 25 °C. Inductively coupled plasma-optical emission spectrometry (ICP-OES) and bicinchonic acid (BCA) protein assays of **L-Pd^{II}·apo-rHLFr** indicate the presence of 37 ± 3 Pd atoms/apo-rHLFr. The same analyses of **I-Pd^{II}·apo-rHLFr** and **H-Pd^{II}·apo-rHLFr** also

(15) Wade, V. J.; Levi, S.; Arosio, P.; Treffry, A.; Harrison, P. M.; Mann, S. *J. Mol. Biol.* **1991**, *221*, 1443–1452.
(16) Barnes, C. M.; Theil, E. C.; Raymond, K. N. *Proc. Natl. Acad. Sci. U.S.A.* **2002**, *99*, 5195–5200.
(17) Meldrum, F. C.; Heywood, B. R.; Mann, S. *Science* **1992**, *257*, 522–523.
(18) Douglas, T.; Stark, V. T. *Inorg. Chem.* **2000**, *39*, 1828–1830.
(19) Klem, M. T.; Mosolf, J.; Young, M.; Douglas, T. *Inorg. Chem.* **2008**, *47*, 2237–2239.
(20) Klem, M. T.; Resnick, D. A.; Gilmore, K.; Young, M.; Idzerda, Y. U.; Douglas, T. *J. Am. Chem. Soc.* **2007**, *129*, 197–201.
(21) Ensign, D.; Young, M.; Douglas, T. *Inorg. Chem.* **2004**, *43*, 3441–3446.
(22) Kim, I.; Hosein, H. A.; Strongin, D. R.; Douglas, T. *Chem. Mater.* **2002**, *14*, 4874–4879.
(23) Iwahori, K.; Yoshizawa, K.; Muraoka, M.; Yamashita, I. *Inorg. Chem.* **2005**, *44*, 6393–6400.
(24) Yamashita, I.; Hayashi, J.; Hara, M. *Chem. Lett.* **2004**, *33*, 1158–1159.
(25) Okuda, M.; Iwahori, K.; Yamashita, I.; Yoshimura, H. *Biotechnol. Bioeng.* **2003**, *84*, 187–194.
(26) Dominguez-Vera, J. M.; Colacio, E. *Inorg. Chem.* **2003**, *42*, 6983–6985.
(27) Ueno, T.; Suzuki, M.; Goto, T.; Matsumoto, T.; Nagayama, K.; Watanabe, Y. *Angew. Chem., Int. Ed.* **2004**, *43*, 2527–2530.
(28) Harrison, P. M.; Artymiuk, P. J.; Ford, G. C.; Lawson, D. M.; Smith, J. M. A.; Treffry, A.; White, J. L. In *Biomineralization*; Mann, S., Webb, J., Williams, R. J. P., Eds.; VCH: Weinheim, 1989; pp 257−294.
(29) Lawson, D. M.; Artymiuk, P. J.; Yewdall, S. J.; Smith, J. M. A.; Livingstone, J. C.; Treffry, A.; Luzzago, A.; Levi, S.; Arosio, P.; Cesareni, G.; Thomas, C. D.; Shaw, W. V.; Harrison, P. M. *Nature* **1991**, *349*, 541–544.
(30) Hempstead, P. D.; Hudson, A. J.; Artymiuk, P. J.; Andrews, S. C.; Banfield, M. J.; Guest, J. R.; Harrison, P. M. *FEBS Lett.* **1994**, *350*, 258–262.
(31) Trikha, J.; Theil, E. C.; Allewell, N. M. *J. Mol. Biol.* **1995**, *248*, 949–967.
(32) Crichton, R. R.; Herbas, A.; ChavezAlba, O.; Roland, F. *J. Biol. Inorg. Chem.* **1996**, *1*, 567–574.
(33) Granier, T.; Comberton, G.; Gallois, B.; d'Estaintot, B. L.; Dautant, A.; Crichton, R. R.; Precigoux, G. *Proteins: Struct., Funct., Genet.* **1998**, *31*, 477–485.
(34) Chasteen, N. D.; Harrison, P. M. *J. Struct. Biol.* **1999**, *126*, 182–194.
(35) Granier, T.; d'Estaintot, B. L.; Gallois, B.; Chevalier, J. M.; Precigoux, G.; Santambrogio, P.; Arosio, P. *J. Biol. Inorg. Chem.* **2003**, *8*, 105–111.
(36) Hempstead, P. D.; Yewdall, S. J.; Fernie, A. R.; Lawson, D. M.; Artymiuk, P. J.; Rice, D. W.; Ford, G. C.; Harrison, P. M. *J. Mol. Biol.* **1997**, *268*, 424–448.
(37) Toussaint, L.; Bertrand, L.; Hue, L.; Crichton, R. R.; Declercq, J. P. *J. Mol. Biol.* **2007**, *365*, 440–452.
(38) Barnes, C. M.; Petoud, S.; Cohen, S. M.; Raymond, K. N. *JBIC, J. Biol. Inorg. Chem.* **2003**, *8*, 195–205.
(39) Butts, C. A.; Swift, J.; Kang, S. G.; Di Costanzo, L.; Christianson, D. W.; Saven, J. G.; Dmochowski, I. J. *Biochemistry* **2008**, *47*, 12729–12739.
(40) Kauko, A.; Pulliainen, A. T.; Haataja, S.; Meyer-Klaucke, W.; Finne, J.; Papageorgiou, A. C. *J. Mol. Biol.* **2006**, *364*, 97–109.
(41) Ceolin, M.; Galvez, N.; Sanchez, P.; Fernandez, B.; Dominguez-Vera, J. M. *Eur. J. Inorg. Chem.* **2008**, *79*, 5–801.
(42) Zeth, K.; Offermann, S.; Essen, L. O.; Oesterhelt, D. *Proc. Natl. Acad. Sci. U.S.A.* **2004**, *101*, 13780–13785.
(43) Alexeev, D.; Zhu, H. Z.; Guo, M. L.; Zhong, W. Q.; Hunter, D. J. B.; Yang, W. P.; Campopiano, D. J.; Sadler, P. J. *Nat. Struct. Biol.* **2003**, *10*, 297–302.
(44) Schemberg, J.; Schneider, K.; Demmer, U.; Warkentin, E.; Muller, A.; Ermler, U. *Angew. Chem., Int. Ed.* **2007**, *46*, 2408–2413.
(45) Sarikaya, M.; Tamerler, C.; Jen, A. K. Y.; Schulten, K.; Baneyx, F. *Nat. Mater.* **2003**, *2*, 577–585.
(46) Abe, S.; Niemeyer, J.; Abe, M.; Takezawa, Y.; Ueno, T.; Hikage, T.; Erker, G.; Watanabe, Y. *J. Am. Chem. Soc.* **2008**, *130*, 10512–10514.

Table 1. Quantitative Analyses of Pd Atoms of **Pd^{II}·apo-rHLFrs** and **Pd^{II}·apo-H49A-rHLFrs**

reaction conditions ([Pd^{2+}]/[apo-rHLFr])	total number of Pd Atoms and Pd binding sites in Pd^{II}· apo-rHLFr: Pd atoms determined by ICP-OES and BCA assay	Pd binding sites determined by crystal structural analyses: interior	exterior
50:1	37 ± 3 (1.5)[a]	144 (6)[a]	0
100:1	88 ± 3 (3.7)[a]	192 (8)[a]	24(1)[a]
200:1	193 ± 10 (8.0)[a]	216 (9)[a]	24(1)[a]
200:1 (apo-H49A-rHLFr)	204 ± 13 (8.5)[a]	168 (7)[a]	24(1)[a]
500:1	365 ± 10 (15)[a]	—[b]	—[b]

[a] The number of Pd atoms/subunit is shown in parentheses. [b] Failure of crystallization.

indicated 88 ± 3 and 193 ± 10 Pd atoms per apo-Fr, respectively (Table 1). **H-Pd^{II}·apo-H49A-rHLFr**, which was prepared by the same procedure, contained 204 ± 13 Pd atoms (Table 1). Crystallization of these composites was performed using a hanging drop vapor diffusion method with $(NH_4)_2SO_4$ and $CdSO_4$ as precipitants in Tris/HCl buffer as described in our previous report.[46]

Whole Structures of Pd^{II}·apo-rHLFrs. To elucidate the binding sites of the metal ions in detail, the crystal structures of **L-Pd^{II}·apo-rHLFr**, **I-Pd^{II}·apo-rHLFr**, and **H-Pd^{II}·apo-rHLFr** have been refined to resolutions of 1.65, 2.10, and 2.50 Å, respectively (Figure 1).[47] Their crystallographic data and refinement statistics are listed in Tables S1 and S2, respectively. We have solved two individual crystal structures for each loading condition to confirm the reproducibility of the anomalous density maps. The highest resolution structures have been chosen for the analysis under each loading condition. The overall structures of the **Pd^{II}·apo-rHLFrs** are essentially identical to that of Pd^{II}-free·apo-Fr.[36] The root-mean-square deviations (rmsds) for C_α's from the Pd^{II}-free·apo-rHLFr are 0.37, 0.48, and 0.61 for **L-**, **I-**, and **H-Pd^{II}·apo-rHLFrs**, respectively.[36] We have discriminated the Pd atoms from the Cd atoms, which are essential for the crystallization of the composites, by using anomalous difference maps in which data sets from a single crystal were collected at 0.5086 and 0.4639 Å of the peak wavelength of Pd and Cd atoms, respectively. One Cd atom per apo-rHLFr subunit was found at the binding site of Asp80, which is located on the outer surface of each of the **Pd^{II}·apo-rHLFrs**. This preserves the intermolecular contacts of apo-rHLFr molecules in crystals as previously reported.[29] Although Fe(II) or Fe(III) atoms bound to the interior surfaces of apo-Frs are displaced by crystallizing cations such as Cd(II) and Tb(III),[28] this is not the case for **Pd^{II}·apo-rHLFrs**; Cd(II) ions observed at the interior surface of **L-** and **H-Pd^{II}·apo-rHLFrs** are bound to different sites from those of Pd(II) ions as shown in Figure 1b and d. This may be rationalized by an extremely slow rate of ligand exchange of Pd(II) ion relative to that of Cd(II) ion.[48] The anomalous difference Fourier maps of **L-Pd^{II}·apo-rHLFr** indicate the existence of 24 Cd binding sites (1 site/subunit) and 144 Pd binding sites (6 sites/subunit) on the interior surface of apo-Fr with a low occupancy of Pd atoms. The Pd atoms in the monomer protein subunit of **L-Pd^{II}·apo-rHLFr** are located in two areas: the 3-fold axis channel and the accumulation center, which consists of Cys48, His49, Glu45, Arg52, and Glu53 (Figure 2b and j). There are 216 and 240 Pd binding sites (9 and 10 sites/subunit) in **I-** and **H-Pd^{II}·apo-rHLFr**, respectively (Figures 1c,d, 2c,d). **I-Pd^{II}·apo-rHLFr** shows three new Pd binding sites with respect to **L-Pd^{II}·apo-rHLFr**. These binding sites are located at the accumulation center and at the N terminus on the exterior surface (Figure 2c and k). Two additional Pd binding sites appear near a crevasse located between the B and D helices of **H-Pd^{II}·apo-rHLFr** (Figure 2d). The quantity of Pd binding sites is larger than the quantity determined by ICP-OES and the BCA assay for each **Pd^{II}·apo-rHLFr**. This observation will be discussed in further detail later.

3-Fold Channel. The 3-Fold channel that consists of highly conserved residues His114, Cys126, Asp127, and Glu130 represents an entrance of metal ions into the Fr cage.[28,35,36] Crystal structures of Frs indicate that various metal ions, such as Ca(II), Cd(II), Zn(II), and Tb(III), are able to bind to the 3-fold channel.[28,29,36] The PdL1−PdL3 atoms in **L-Pd^{II}·apo-rHLFr** interact with three conserved residues His114, Cys126, and Glu130 (Figure 2f). In particular, the observation of two different conformations of the Cys126 side chain indicates that there are at least two coordination structures for Cys126 to ligate to either PdL1, PdL2, or PdL3. In the 3-fold channel of **I-Pd^{II}·apo-rHLFr**, three Pd atoms remain in the same region, although their locations are somewhat different from those identified in **L-Pd^{II}·apo-rHLFr**, which has broader anomalous electron densities than those of **L-Pd^{II}·apo-rHLFr** as shown in Figure 2f and g. **H-Pd^{II}·apo-rHLFr** holds two Pd atoms in this region, while electron density is missing from the side chain of Glu130 as a result of conformational flexibility (Figure 2h). The low resolution of the **H-Pd^{II}·apo-rHLFr** data set might be responsible for the decreased number of Pd atoms observed at the 3-fold channel.

Accumulation Center and Additional Sites. As shown in Figure 2, Pd binding sites are found in the accumulation center, which includes Glu45, Cys48, His49, Arg52, and Glu53 residues located near the proposed ferrihydrate site where a number of Cd(II) and Tb(III) ions are preferably bound.[28,33,36] Three Pd sites (PdL4−PdL6) of **L-Pd^{II}·apo-rHLFr** are observed at the accumulation center (Figure 2j). Interestingly, PdL5 and PdL6 exhibit a thiol-bridged dinuclear structure with Cys48, while a single cadmium atom is located at the same binding site in Pd^{II}-free·apo-rHLFr (Figure 2i).[33,36] The coordination structure of the dinuclear site is similar to a typical Pd thiol-bridged dinuclear complex[50] and appears to be stabilized by the coordination of Glu45 and water molecules (Figure 2j), although the Glu45 side chain adopts two conformations. The anomalous difference map of **I-Pd^{II}·apo-rHLFr** reveals two additional Pd binding sites, PdI7 and PdI8, located between PdI4 and the dinuclear site (PdI5 and PdI6) at the accumulation center (PdI7 and PdI8, Figure 2k). On the exterior surface, PdI9 interacts with several residues at the N-terminal region and Asp40 of an adjacent subunit

(47) Atomic coordinates are deposited in the Protein Data Bank under accession numbers 2Z5P, 2Z5Q, 2Z5R, and 3FI6 for **L-Pd^{II}·apo-rHLFr**, **I-Pd^{II}·apo-rHLFr**, **H-Pd^{II}·apo-rHLFr**, and **H-Pd^{II}·apo-H49A-HLFr**, respectively.

(48) Richens, D. T. *The Chemistry of Aqua Ions*; Wiley: West Sussex, 1997.

(49) The residues, His49 and Glu130 of **I-Pd^{II}·apo-rHLFr**, His49, Arg52, Cys126, and Glu130 of **H-Pd^{II}·apo-rHLFr**, and Cys126, Asp127, and Glu130 of **H-Pd^{II}·apo-H49ArHLFr**, were replaced by Ala because electron densities of these side chains are missing. The side chains of Glu45, Glu53, Glu56, and Cys126 of **L-Pd^{II}·apo-rHLFr**, Arg52 of **I-Pd^{II}·apo-rHLFr**, Glu45 of **H-Pd^{II}·apo-rHLFr**, Asp38, Arg52, and Glu53 of **H-Pd^{II}·apo-H48A-rHLFr**, and Arg52 and Glu56 of Pd^{II}(allyl)·apo-rHLFr were revealed as dual conformers.

(50) Osakada, K.; Ozawa, Y.; Yamamoto, A. *J. Organomet. Chem.* **1990**, *399*, 341–348.

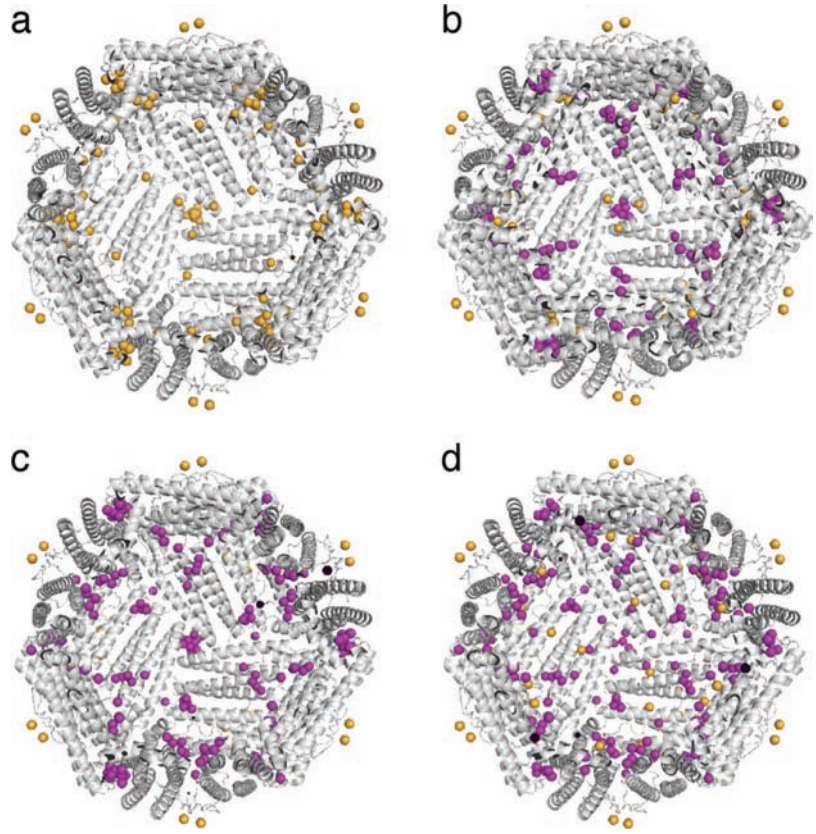

Figure 1. The whole structures of Pd^{II}-free and **Pd^{II}·apo-rHLFrs**. (a) Pd^{II}-free·apo-rHLFr has 120 Cd binding sites on the interior surface and 24 Cd binding sites on the exterior surface (PDB ID 1AEW). (b) **L-Pd^{II}·apo-rHLFr** has 144 Pd and 24 Cd binding sites on the interior surface. There are 24 other Cd binding sites on the exterior surface. (c) **I-Pd^{II}·apo-rHLFr** has 192 Pd binding sites on the interior surface. On the exterior surface, additional 24 Pd binding sites are located in the vicinity of Ser2, and 24 Cd binding sites are located near Asp80. (d) **H-Pd^{II}·apo-rHLFr** has 216 Pd binding sites on the interior surface as well as 24 Cd and 24 Pd binding sites on the exterior surface. (a)−(d) are depicted along 3-fold axes. The Pd and Cd atoms are indicated as sphere models colored purple and orange, respectively.

(Figure 2c). The structure of **I-Pd^{II}·apo-rHLFr** exhibits large differences in side-chain conformations of Glu45 and Arg52 relative to those of **L-Pd^{II}·apo-rHLFr**. In addition, the electron density of the imidazole ring is missing from His49. The side chain of Glu45 is expected to interact with PdI7 and PdI8 to stabilize the deposition of these ions at the accumulation center, while no significant changes were observed in the coordination structures of PdI5 and PdI6 with Cys48 (Figure 2k). Although **H-Pd^{II}·apo-rHLFr** shows no large changes in the coordination geometry observed at the accumulation center relative to **I-Pd^{II}·apo-rHLFr**, the two strong anomalous densities of Pd atoms, PdH8 and PdH9 (>4σ) with coordination to Arg64 and His124, respectively, are found near a crevasse located between the B and D helices (Figure 2d). The results indicate that the accumulation center first becomes occupied by five Pd atoms, followed by additional binding of Pd atoms to the sites of PdH8 and PdH9 (Figure 2d).

Crystal Structure of H-Pd^{II}·apo-H49A-rHLFr. To elucidate the accumulation of Pd(II) ions at the accumulation center in detail, the crystal structure of **H-Pd^{II}·apo-H49A-rHLFr** has been determined with 1.8 Å resolution (Figure 3).[47] The crystallographic data and refinement statistics are listed in Tables S1 and S2, respectively. The overall structure is essentially identical to that of Pd^{II}-free·apo-Fr and **H-Pd^{II}·apo-rHLFr** (rmsds in C_α atoms: 0.42 and 0.61, respectively) (Figure 3a and b).[36] One Cd atom per **H-Pd^{II}·apo-H49A-rHLFr** subunit was found at the binding site of Asp80, which is located on the outer surface as observed in **Pd^{II}·apo-rHLFrs** (Figure 1). The whole structure shows 168 and 24 Pd binding sites on the interior and exterior surfaces of apo-H49A-rHLFr, respectively (Figure 3a and b). They are located at the 3-fold channel, the accumulation center, and other binding sites with coordination to Ser2 and His124 as found in **H-Pd^{II}·apo-rHLFr**, along with a new binding site of His173 on the interior surface (Figure 3b). The coordination structures of PdHHis1 and PdHHis2 binding to His114 and Cys126 in the 3-fold channel are almost identical to that of **H-Pd^{II}·apo-rHLFr** (Figure 3c and e). Electron densities of side chains of Asp127 and Glu130 are missing as found in **H-Pd^{II}·apo-rHLFr**. At the accumulation center, no electron densities of Pd atoms have been found around His49Ala in **H-Pd^{II}·apo-H49A-rHLFr**, while the PdH3, PdH6, and PdH7 are observed at the center for **H-Pd^{II}·apo-rHLFr**(Figure 3d and f). The anomalous density maps of three Pd atoms, PdHHis3, PdHHis4, and PdHHis5, are observed immediately above the sulfur atom of Cys48 with the Pd−S distances of 2.36, 2.17, and 2.54 Å, respectively, while other **Pd^{II}·apo-rHLFrs** give dinuclear structures at the same site. This trinuclear core is a distorted structure as compared to a reported trinuclear palladium alkanethiolate complex.[51] We need further investigation to elucidate the different cluster formation in apo-rHLFr and apo-H49A-rHLFr.

(51) Espinet, P.; Hernandez, C.; Martin-Alvarez, J. M.; Miguel, J. A. *Inorg. Chem.* **2004**, *43*, 843–845.
(52) Zhang, L.; Swift, J.; Butts, C. A.; Yerubandi, V.; Dmochowski, I. J. *J. Inorg. Biochem.* **2007**, *101*, 1719–1729.

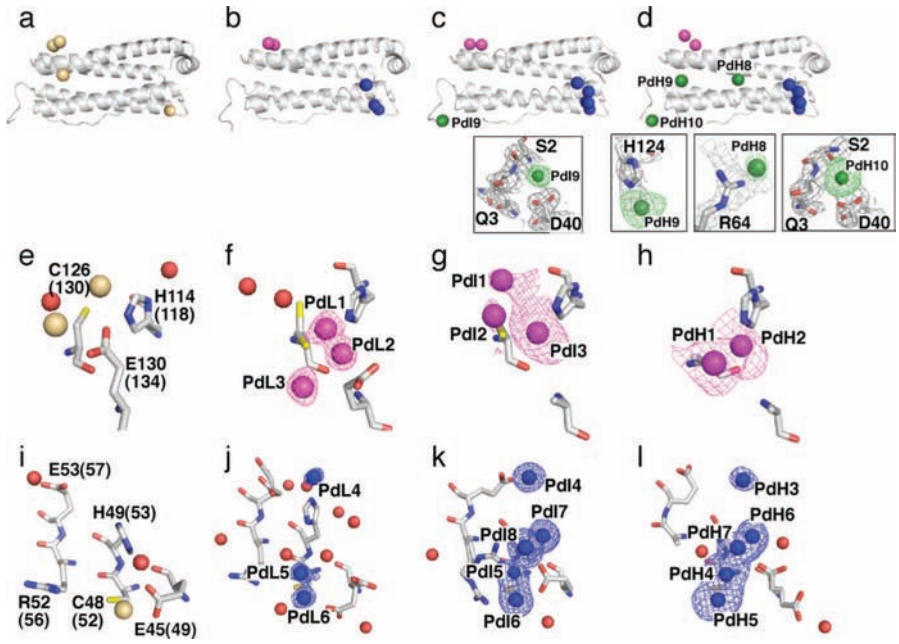

Figure 2. The binding site structures of Pd^{II}-free·apo-rHLFr and **Pd^{II}·apo-rHLFrs**. (a−d) Monomer unit structures of Pd^{II}-free·apo-rHLFr, **L-**, **I-**, and **H-Pd^{II}·apo-rHLFr**, respectively.[49] (e−h) 3-fold channel structures of Pd^{II}-free·apo-rHLFr, **L-**, **I-**, and **H-Pd^{II}·apo-rHLFr**, respectively. (i−l) Accumulation center structures of Pd^{II}-free·apo-rHLFr, **L-**, **I-**, and **H-Pd^{II}·apo-rHLFr**, respectively. The Pd^{II}-free·apo-rHLFr structure is taken from PDB ID 1AEW.[36] Pd atoms in **L-**, **I-**, and **H-Pd^{II}·apo-rHLFrs** are shown as **Pd**Ls, **Pd**Is, and **Pd**Hs, respectively. The Pd atoms in the 3-fold axis channels, accumulation centers, and the third site are colored purple, blue, and green, respectively. Cd atoms are indicated as pale yellow spheres. The O atoms of water molecules are shown as red spheres. Anomalous difference Fourier maps at 4.0σ indicating the positions of individual palladium atoms are shown as purple and blue spheres. The insets of (c) and (d) are close-up views of PdI9, PdH8, PdH9, and PdH10. The original residue numbers of Pd^{II}-free·apo-rHLFr are given in parentheses (e and i).[36]

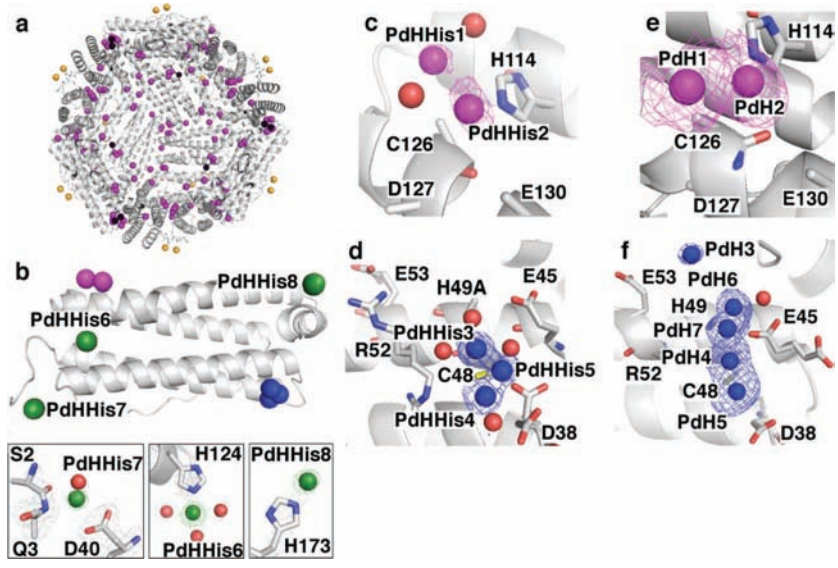

Figure 3. The crystal structure of **H-Pd^{II}·apo-H49A-rHLFr**.[49] (a) The whole structure has 168 Pd binding sites on the interior surface. Additionally, 24 Pd binding sites are located in the vicinity of Ser2, and 24 Cd binding sites are located near Asp80 on the exterior surface. These views are along the 3-fold axis. The Pd and Cd atoms are indicated as sphere models colored purple and orange, respectively. (b) Monomer unit structure of **H-Pd^{II}·apo-H49A-rHLFr**. The insets are close-up views of PdHHis6−9. (c and e) 3-fold channel structures of **H-Pd^{II}·apo-H49A-rHLFr** and **H-Pd^{II}·apo-rHLFr**, respectively. (d and f) Accumulation center structures of **H-Pd^{II}·apo-H49A-rHLFr** and **H-Pd^{II}·apo-rHLFr**, respectively. Pd atoms in **H-Pd^{II}·apo-H49A-rHLFr** and **H-Pd^{II}·apo-rHLFrs** are shown as **PdHHis**s and **PdH**s, respectively. The Pd atoms in the 3-fold axis channels, accumulation centers, and the third site are colored purple, blue, and green, respectively. Cd atoms are indicated as pale yellow spheres. The O atoms of water molecules are shown as red spheres. Anomalous difference Fourier maps at 4.0σ indicating the positions of individual palladium atoms are shown as purple and blue spheres.

Comparison of L-Pd^{II}·apo-rHLFr with Pd^{II}-free· and Pd(allyl)·apo-rHLFr. The whole structure of the apo-rHLFr cage was not affected by the coordination of Pd(II) ions because the rmsd values in C_α atoms of **L-Pd^{II}·apo-rHLFr** are 0.37 and 0.44 from Pd^{II}-free·apo-rHLFr and Pd^{II}(allyl)·apo-rHLFr, respectively.[36,46] However, conformation of amino acid side chains is changed by the Pd^{II} binding at the Pd binding areas as shown in Figure 4.[36] At the 3-fold channel, the side-chain conformations of Cys126 and Glu130 are altered to retain the coordination of Pd^{II}(allyl) complexes and Pd(II) ions as compared to those in Pd^{II}-free·apo-rHLFr (Figure 4a−c). Interestingly, Glu130 in **L-Pd^{II}·apo-rHLFr** ligates to the PdL2 atom,

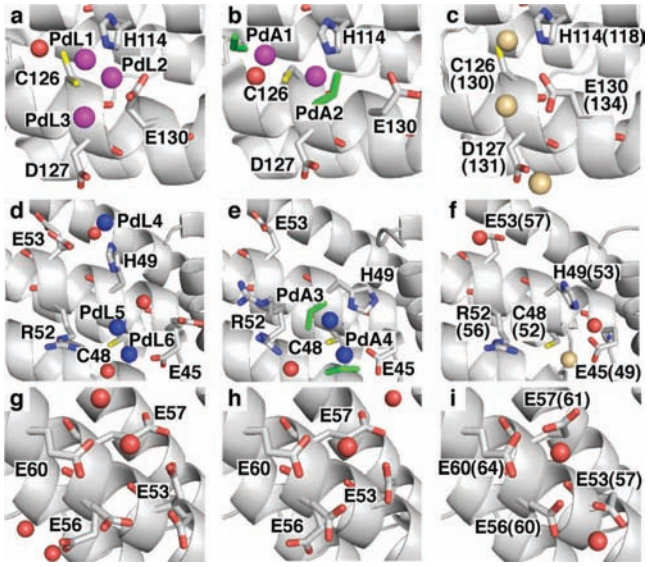

Figure 4. Binding site structures of **L-Pd^{II}·**, Pd^{II}(allyl)·, and Pd^{II}-free·apo-rHLFr.[49] (a−c) 3-fold channel of **L-Pd^{II}·**, Pd^{II}(allyl)·, and Pd^{II}-free·apo-rHLFr, respectively. (d−f) Accumulation center of **L-Pd^{II}·**, Pd^{II}(allyl)·, and Pd^{II}-free·apo-rHLFr, respectively. (g−i) Ferrihydrite nucleation center of **L-Pd^{II}·**, Pd^{II}(allyl)·, and Pd^{II}-free·apo-rHLFr, respectively. The Pd^{II}(allyl)· and Pd^{II}-free·apo-rHLFr structures are taken from PDB IDs 2ZG7 and 1AEW, respectively.[36,46] Pd atoms in **L-Pd^{II}·** and Pd^{II}(allyl)·apo-rHLFr are shown as **PdL**s and **PdA**s, respectively. The Pd atoms in the 3-fold axis channels and accumulation centers are colored purple and blue, respectively. Cd atoms are indicated as pale yellow spheres. The O atoms of water molecules are shown as red spheres. The allyl ligands of Pd^{II}(allyl)·apo-rHLFr are shown as green tube models. The original residue numbers of Pd^{II}-free·apo-rHLFr are given in parentheses (c, f, and i).[36]

while the side chain in Pd^{II}(allyl)·apo-rHLFr is displaced by steric hindrance of the allyl ligand of the Pd^{II}(allyl) complex bound to His114 and Cys126 (Figure 4a and b). His114 and Asp127, which are well conserved and bound to metal ions,[36] show no structural perturbation regardless of whether the Pd(II) ions coordinate to them or not. The same rigid conformations of His114 and Asp127 have been found in amphibian red-cell L-Fr containing Mn(II) and Mg(II) ions.[31] Therefore, our results suggest that the conformation changes of Cys126 and Glu130 play crucial roles for metal bindings at the 3-fold channel to transport metal ions into the apo-rHLFr cage. The conformation of His49 is dramatically changed by the coordination of Pd(II) ions at the accumulation center (Figure 4d−f). While the imidazole group of His49 was bound to a Pd^{II}(allyl) complex ligated to Cys48 to maintain the dinuclear structure of Pd^{II}(allyl)-S(Cys48)-Pd^{II}(allyl) of Pd^{II}(allyl)·apo-rHLFr (Figure 4e), the same imidazole ring in L-Pd^{II}·apo-rHLFr was oriented to the opposite direction due to the coordination with PdL4 (Figure 4d and e). In contrast, at the ferrihydrite nucleation site, the side-chain conformations of four well-conserved glutamic acids, Glu53, Glu56, Glu57, and Glu60, were almost identical among the three crystal structures (Figure 4g−i).

Accumulation Mechanism of Pd(II) Ions. It is known that many different metal ions can occupy the apo-Fr cage through the 3-fold channels. These metal ions are expected to first accumulate at the negatively charged interior regions by coordination of the carboxylate groups of glutamic acid residues and are then mineralized either by oxidation or by ligation to inorganic anions.[28,34,52] The X-ray crystal structures and mutagenesis investigations of apo-Frs show that the metal ions such as Cd(II), Zn(II), Mn(II), and Tb(III) are located at the ferrihydrite nucleation sites, which consist of Glu53, Glu56, Glu57, and Glu60.[28,31−37] In contrast, our results show that Pd binding sites are located at different regions, which include Glu45, Cys48, His49, Arg52, and Glu53 (accumulation center) (Figures 2 and 3). Pd(II) ions generally form square planar complexes, while Cd(II), Zn(II), and Mn(II) prefer octahedral coordination structures, which are similar to Fe(II) ion.[48,53] Cys48 is expected to be crucial to retain the square planar geometry of Pd(II) ions by the formation of a di- or trinuclear structure with cooperative ligation of Glu45 and water molecules (Figures 2j and 3d). In contrast, four well-conserved glutamic acid residues at the ferrihydrite nucleation center have a greater tendency to promote octahedral geometry as found for Cd(II) ions in the crystal structure of mouse L-chain ferritin.[35] Moreover, the accumulation center has relatively high *B*-factors for side chains of amino acid residues, while electrostatic potentials of apo-Fr calculated by GRASP[54] show that the 3-fold channel and the ferrihydrite nucleation site are more negatively charged regions than the accumulation center (Figure 5).[54] Therefore, the results suggest that Pd(II) ions selectively bind to Cys48 and His49 at the accumulation center with square planar geometry instead of the ferrihydrite nucleation center consisting of highly conserved glutamic acid residues to preserve octahedral coordination geometry.

A series of crystal structures of **Pd^{II}·apo-rHLFrs** containing different amounts of Pd(II) ions indicates that there are two deposition areas located in the 3-fold channel and at the accumulation center (Figure 2). There is a large difference in the number of Pd atoms estimated by ICP-OES and BCA assay (1.5 Pd atoms/subunit) from that of the crystal structure (6 Pd atoms/subunit) of **L-Pd^{II}·apo-rHLFr** (Table 1). Moreover, His49 gives weaker electron density with increasing number of Pd(II) ions at the accumulation centers of Pd^{II}·apo-rHLFrs (Figure 2i−l). With respect to **H-Pd^{II}·apo-H49A-rHLFr**, the number of Pd atoms obtained by quantitative analysis is almost identical to that of the crystal structure (Table 1). The crystal structure of **H-Pd^{II}·apo-H49A-rHLFr** shows all of the Pd atoms being observed with higher occupancy than those of all **Pd^{II}·apo-rHLFrs**. At an early stage of Pd(II) accumulation in the apo-rHLFr cage, Pd(II) ions are expected to bind to any of the sites of the two areas in several possible binding modes. Therefore, all of the Pd atoms in apo-rHLFr are superimposed on the one subunit with low occupancy of the electron density. The conformational changes of His49 and the surrounding residues, Glu45 and Arg52, stabilize the Pd(II) ion binding and promote an increase in the number of Pd atoms bound to the accumulation center (Figure 2j−l). Furthermore, Cys48 is a key residue for the formation of a Pd dinuclear coordination structure during the accumulation of Pd(II) ions.

When apo-rHLFr was treated with a large excess of Pd(II) ions (500 equiv of K_2PdCl_4), only 365 Pd(II) ions were accommodated in apo-rHLFr (Table 1). Upon addition of a large quantity of Pd(II) ions, all of the binding sites are fully occupied by Pd(II) ions accompanied by conformational changes of amino acid side chains as shown in a series of coordination structures of **L-**, **I-**, and **H-Pd^{II}·apo-rHLFrs** (Figure 2). Preparation of 2.0 ± 0.3 nm Pd nanoparticles with a narrow size distribution in apo-HSFr is reasonably attributed to a limited number of

(53) Lippard, S. J.; Berg, J. M. *Principles of Bioinorganic Chemistry*; University Science Books: Mill Valley, 1994.
(54) Gallois, B.; d'Estaintot, B. L.; Michaux, M.-A.; Dautant, A.; Granier, T.; Précigoux, G.; Soruco, J.-A.; Roland, F.; Chavas-Alba, O.; Herbas, A.; Crichton, R. R. *J. Biol. Inorg. Chem.* **1997**, *2*, 360–367.

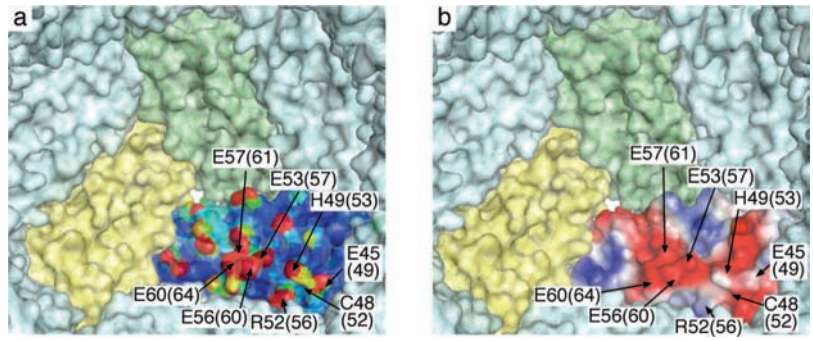

Figure 5. The molecular surfaces of apo-rHLFr subunit in 24mer (PDB ID 1AEW) are colored with B-factor (a) and electrostatic potentials (b).[36] The surface of a monomer for (a) is colored with red to blue for large to small *B*-factor values of each atom. Part (b) is colored with red to blue for negative to positive charge of each residue. The original residue numbers of Pd^{II}-free·apo-rHLFr are given in parentheses.[36] (a) and (b) are depicted along 3-fold axes. Two other monomers composing the 3-fold channel are colored with yellow and green. They are reproduced by Pymol.[56]

Pd(II) ions accumulated on the internal surface of apo-HSFr as reported previously.[27] Moreover, on the basis of these crystal structures, we assume that the single Pd^0 nanoparticle is formed in apo-HSFr by assembly of small Pd^0 seeds generated at each accumulation center within the 24mer cage upon the reduction of Pd(II) ions by $NaBH_4$ as proposed for the formation of cobalt oxide nanoparticles in apo-HSFr.[55]

Conclusion

We have identified two specific binding areas of Pd(II) ions and analyzed dynamic coordination changes by a combination of the crystal structure and ICP-OES quantitative analyses of apo-rHLFr and the mutant containing low, intermediate, and high content of Pd(II) ions. These results suggest that Pd(II) ions are likely to bind to these binding areas with several binding modes at an early stage of Pd(II) accumulation. We recently published a report on the deposition of Pd^{II}(allyl) complexes on the interior surface of apo-rHLFr.[46] The complexes are exclusively bound to two specific sites by utilizing Cys48 and Cys126. The binding sites and binding structures of Pd(II) ions depend on the absence or presence of external ligand such as an allyl molecule. Our results provide intriguing implications not only for the fundamental role of protein−metal ion interactions but also for the design of new inorganic materials using protein scaffolds. On the basis of these findings, further design of nanoparticles using protein cages is in progress to improve the catalytic reactivity.

Acknowledgment. We thank members of BL38B1 and BL41XU of SPring-8 for assistance during the diffraction data collection. This work was supported by a grant from the 21st Century- and Global-COE programs of Nagoya University for S.A., a JSPS Research Fellowship for Young Scientist for M.S., and Grant-in-Aid for Scientific Research (Grant Nos. 17655076 and 18685019 for T.U.) and on Priority Areas (Grant No. 16033226, Chemistry of Coordination Space for Y.W.) from the Ministry of Education, Culture, Sports, Science, and Technology, Japan, and PRESTO, Japan Science and Technology Agency (JST). Synchrotron radiation experiments were conducted under the approval of 2006A1782 and 2007A1001 at SPring-8.

Supporting Information Available: Tables S1 and S2 and experimental procedures. This material is available free of charge via the Internet at http://pubs.acs.org.

JA806688S

(55) Kim, J. W.; Choi, S. H.; Lillehei, P. T.; Chu, S. H.; King, G. C.; Watt, G. D. *Chem. Commun.* **2005**, 4101–4103.
(56) http://pymol.sourceforge.net/.